Combined Methodology for Accurate Evaluation of Distance and Direction of Chromaticity Shifts in LED Reliability Tests

Simon Benkner, Sebastian Babilon, Alexander Herzog, Tran Quoc Khanh

***Abstract*—Light Emitting Diodes are an integral part of modern illumination systems. While their long-term stability in terms of lumen maintenance used to be in the focus leading to drastically increased nominal lifetimes over the past decade, the color shift or respectively chromaticity shift is lately attracting more and more attention especially in lighting applications that demand for a high chromatic stability. Common ways of displaying and reporting color shifts in LEDs and LED products provide only limited possibilities to accuratly classify changes in color according to the current understanding of the underlying degradation processes. This paper therefore presents a methodology to overcome the observed discrepancies in analyzing time-dependent chromaticity data in terms of their shift direction and distance within the CIE 1976 (u', v') chromaticity diagram. The use of an extrapolation function extending the shift towards the spectral locus enables the determination of the corresponding nearest spectral locus intersection wavelength. Thereby, it is possible to classify changes in color according to different shift regions, which basically allows for performing an automated comprehensive color shift mode analysis. As part of this paper five different algorithmic approaches for determining the intersection wavelength and shift region are discussed and compared in terms of their accuracy and ease in implementation.**

***Index Terms*—Color Shift, Chromaticity Shift, Light Emitting Diode (LED), Lifetime Measurements, Color Stability, Reliability.**

I. Introduction

LIGHT emitting diodes (LEDs) have found their way into almost every area of modern lighting design and application (see e.g., [1]–[8]). Aside from their compact form factors, high efficiencies, and extensive control features, the long product life time of LEDs constitutes one of their key advantages. Since the early days of adoption, the LEDs' durability has been greatly improved – 50 000 h and more are often claimed by manufacturers of modern LED products [9], which manifests a huge increase in life time compared to most conventional light sources.

In contrast to the latter, the end of life for LEDs and corresponding luminaires is usually not characterized by a total loss of light emission. Instead, a steady decline in luminous flux as well as a slow but continuous shift in chromaticity occur up to the point where an unacceptably low light emission or a too large change in perceived color represent functional failure [10]. Several different modes and mechanisms of LED failure related to the semiconductor, the interconnects, and the package itself have been identified in the literature. A detailed review including a discussion on failure causes, characteristics and implications is given by Chang *et al.* [11].

So far, discussions about the durability of LED were mainly driven by the decrease in luminous flux, the so-called lumen maintenance. This has led to the development of a variety of tools, methods and standards for the LED life estimation [12]–[15]. The evaluation of the color shift, on the other hand, has yet been considered only rudimentary in terms of color distance and shift direction. This is confirmed by the absence of applicable standards. In use-cases with a primary focus on visual appreciation and observer preference [16], [17], such as for example in museum or retail lighting, a high degree of color stability is critical, whereas in other cases, like for example in street or automotive lighting, where providing adequate levels of brightness and visibility are the main criteria [18], color maintenance is less important.

Besides the need for such application-related definitions of acceptability limits, the industry further lacks a consensus methodology for accelerated testing, analyzing and subsequent prediction of chromaticity shifts. As of today chromaticity shift evaluation is performed visually on the CIE 1976 (u', v') uniform chromaticity scale (UCS) diagram. Thus, a standardized guide to color maintenance allowing for advanced LED reliability ratings and modelling would be highly appreciated among consumers and manufacturers and may help to develop potential tracking and compensation strategies for LED-based luminaires.

In order to develop such long-term LED color-shift prediction models, it is crucial to gain further knowledge about the nature of the causal degradation processes and potential acceleration factors, such as current, humidity and temperature, affecting chromatic stability. In particular, more detailed information are needed regarding the time dependence of the direction and distance of chromatic changes observed for the emitted light spectrum that may subsequently be correlated with certain chromaticity-shift modes (CSM) and failure mechanisms. In this context, the current paper presents an enhanced methodology for displaying and classifying time-dependent chromaticity shifts in LEDs, which goes beyond the rudimentary documentation that, if at all, is performed by some

S. Benkner, S. Babilon, A. Herzog, and T. Q. Khanh are with the Laboratory of Lighting Technology, Technical University of Darmstadt, Darmstadt, 64289 Germany; e-mail: simon.benkner@tu-darmstadt.de.

S. Babilon is currently on a research fellowship with the Light and Health Research Center, Department of Population Health Science and Policy, Icahn School of Medicine at Mount Sinai, One Gustave L. Levy Place, New York, NY 10029, USA

manufacturers.

II. Colorimetric Basics

The chromatic appearance of an LED (or any other) light source can be characterized by using chromaticity coordinates derived from CIE colorimetry. Assuming that the spectral power distribution of the light source $S_\lambda(\lambda)$ is known in the the visible range of the electromagnetic spectrum, $\lambda_{\mathrm{vis}} = [380\,\mathrm{nm}, 780\,\mathrm{nm}]$, the corresponding CIE tristimulus values can be calculated from

$$X = K \int_{\lambda_{\mathrm{vis}}} S_\lambda(\lambda)\bar{x}(\lambda)\,\mathrm{d}\lambda, \tag{1}$$

$$Y = K \int_{\lambda_{\mathrm{vis}}} S_\lambda(\lambda)\bar{y}(\lambda)\,\mathrm{d}\lambda, \tag{2}$$

$$Z = K \int_{\lambda_{\mathrm{vis}}} S_\lambda(\lambda)\bar{z}(\lambda)\,\mathrm{d}\lambda, \tag{3}$$

where $\bar{x}(\lambda)$, $\bar{y}(\lambda)$, and $\bar{z}(\lambda)$ are the color matching functions of the CIE 1931 2° standard observer with $\bar{y}(\lambda)$ being equal to the luminous efficiency function $V(\lambda)$ and K is an arbitrary scaling factor. In case that $S_\lambda(\lambda)$ is measured in radiometric units, this scaling factor is usually set to the maximum of the luminous efficacy of radiation, $K_{\mathrm{m}} = 683\,\mathrm{lm\,W^{-1}}$, which creates the link to photometry.

The two-dimensional projection of this three-dimensional human-vision-based representation of color sensation yields a pair of chromaticity coordinates that determines the light source's chromatic features, in particular its hue and saturation. This basically defines a unique color impression so that two different light sources with equal chromaticity coordinates should theoretically exhibit the same chromatic appearance regardless of their spectral composition and perceived lightness.

The set of all possible chromaticities being perceived by humans can be visualized in form of so-called chromaticity diagrams whose boundaries are determined by the chromaticity coordinates (i.e., the spectral locus) of monochromatic light stimuli ranging from $380\,\mathrm{nm}$ to $780\,\mathrm{nm}$. After several iterations, in which the way chromatic information is depicted has continuously evolved to better match visual evaluations of color differences, the CIE eventually came up with the CIE 1976 (u', v') UCS, which is still the recommended standard for describing and comparing the chromatic output of light sources.

Corresponding chromaticity coordinates can be calculated from the original tristimulus values of Eqs. (1)–(3) by using the following expressions:

$$u' = \frac{4X}{X + 15Y + 3Z}, \tag{4}$$

$$v' = \frac{9Y}{X + 15Y + 3Z}. \tag{5}$$

The difference in chromaticity between two light sources with coordinates (u'_1, v'_1) and (u'_2, v'_2) is defined as the Euklidean distance

$$\Delta_{u'v'} = \sqrt{(u'_1 - u'_2)^2 + (v'_1 - v'_2)^2}. \tag{6}$$

III. Current State of Chromaticity Shift Evaluation

Basically, there are two different ways of representing chromaticity shifts of LEDs (or any other light source) applied in practice. The first one makes use of the CIE 1976 (u', v') chromaticity diagram, which is adopted for illustrating the chromaticity coordinates of the light source under consideration at two distinct points in time. Sometimes, a visual indication of the shift direction is manually added, e.g., by using an arrow. However, there is no recommended standard yet and manufacturers, in contrast to researchers, rarely use this form to publish chromaticity maintenance data. It is also to be noted that the assignment of a chromaticity shift direction to a certain color range (e.g. blue, green, yellow, red) is currently not standardized in terms of the number color ranges neither are their wavelength boundaries clearly defined. The second, slightly more common way is to calculate the corresponding absolute difference $\Delta_{u'v'}$ between the chromaticity coordinates of the light source at two different times of interest, e.g., t_n and t_{n-1} or t_n and t_0. For instance, the ENERGY STAR® program run by the U.S. Environmental Protection Agency (EPA) demands LED products to not overstep a value of 0.007 $\Delta_{u'v'}$ during corresponding reliability tests. Even though this method allows for estimating the magnitude of the chromaticity shift and whether it is perceivable to humans, potentially important information on the shift direction and thus the underlying degradation cause is obviously lost. [10], [19]

A. Causes of Chromaticity Shift in LEDs

During operation, various mechanisms occurring at different levels within an LED are found to affect the chromaticity of the light being emitted by that device. Although not fully elucidated yet, related failure causes can be categorized according to the directions of the induced chromaticity shifts and with regard to where exactly the degradation takes place. Van Driel *et al.* [20] identified five different regions within the LED that usually suffer from known degradation processes: *Die level (1)*, *phosphor and binder level (2)*, *package level (3)*, *encapsulant level (4)* and *contamination level (5)*. Making use of this level assignment, Table I summarizes the most frequent causes of chromaticity shifts in LEDs sorted by the direction of their corresponding shift vectors.

B. Chromaticity Shift Modes

As part of the device aging process, an LED can undergo multiple shift direction changes during lifetime. Certain behavior characteristics have been derived and classified accordingly into so-called chromaticity shift modes (CSMs). The literature identifies five main CSMs that can reveal additional information about the specific degradation process and the degree of operational stress experienced by the LED device [10], [20]: i) CSM-1 typically involves a continuous shift into

TABLE I
OVERVIEW OF A NUMBER OF POTENTIAL CAUSES LEADING TO CHROMATICITY SHIFTS IN LED PRODUCTS. THE ASSIGNMENT OF SHIFT DIRECTION AND DEGRADATION LEVEL IS BASED ON INFORMATION PROVIDED BY DOE [10] AND VAN DRIEL *et al.* [20]

Direction	Level	Cause
Blue	1	Annealing of epitaxial layer and interconnects increases photon output [20]
	2	Change in refraction index of binder [20]
	2	Drop in phosphor quantum efficiency [20]
	2	Vertical cracking enables blue photon bypassing [10]
	2	Heat induced change in phosphor distribution [10]
	3	Lead frame, reflector and molding compound oxidation in plastic lead leaded chip carrier packages [10]
	5	Moisture ingress leads to swelling of silicone binder and thus decreasing phosphor density [20]
Yellow	1	Dielectric breakdown and electrical contact corrosion increase forward voltage [20]
	2	Cracks and delamination at die-phosphor interface [20]
	2	Chemical changes increase phosphor quantum efficiency [10]
	3	Discoloration and oxidation of optical components like lenses or reflectors [10]
	3	Oxidation of resin and lead frame in PLCC package [20]
	4	Cracks at high temperatures and photon flux in old epoxy encapsulants (before 2008) [20]
	4	Increased blue light absorption due to silicone aging [20]
Green	2	Oxidation of nitride and oxynitride phosphors [20]
Red	2	Decreasing emission of green phosphors [10]

the blue direction, which is expressed by a steady decrease in both chromaticity coordinates u' and v' and favored by low operational stress conditions, such as low LED board temperatures and/or low drive currents; ii) CSM-2 describes a chromaticity shift into the green direction (i.e., decrease in u' at more or less constant v'), which is also favored by low stress conditions and most likely related to oxidation occurring in the phosphor; iii) CSM-3 represents a persistent shift into the yellow direction (v' increases significantly at only slightly changing u') that usually occurs after an initial shift into the blue direction resulting in a characteristic hook pattern when plotted in the chromaticity diagram. This CSM is primarily observed in high-power LEDs, which in the nature of things get frequently exposed to high operational stress conditions leading to delamination and cracking in the phosphor layer; iv) CSM-4 is characterized by a short initial shift into the blue direction, followed by a shift into yellow direction, and a subsequent second shift into the blue direction and is only observed for plastic leaded chip carrier (PLCC) LED packages, e.g., mid-power LEDs, suggesting that oxidation of the molding resin might be the main cause of degradation; v) CSM-5 involves a shift into the red direction expressed by a significant increase in u' at more or less constant v' and relies on similar degradation processes as observed for CSM-3. Such being the case, this CSM also primarily occurs in high-power LEDs.

IV. ENHANCED CHROMATICITY SHIFT EVALUATION

In the attempt of representing the time-dependence of the absolute magnitude of chromaticity shifts in LEDs while retaining the full chromatic information including the classification of shift directions, which, as discussed in the previous section can be related to certain degradation characteristics, an enhanced methodology of chromaticity maintenance will be proposed in the following.

Thinking of the LED's CIE 1976 UCS color coordinates obtained for the ith maintenance measurement as a two-dimensional vector $P_i = (u'_i, v'_i)^T$ in a Cartesian color space, each subset of two sequential chromaticity vectors P_n and P_{n-m} with $n - m \geq 0$ should be transformed to polar coordinates first. Each of these subsets is then evaluated separately. Thus, m is either set to 1 if one is interested in the (relative) shift between two consecutive measurements or to the value of n, i.e., $n - m = 0$, if one is interested in the (absolute) shift between the LEDs initial chromaticity at $t_0 = 0\,\mathrm{h}$ and its nth measurement chromaticity. In any case, P_{n-m} is taken as the new origin of the transformed coordinate space so that $P_n(u'_n, v'_n) \mapsto P'_n(r_s, \phi_s)$, where the shift radius r_s equals the absolute distance in chromaticity coordinates,

$$r_s = \Delta_{u'v'} = \sqrt{(u'_n - u'_{n-m})^2 + (v'_n - v'_{n-m})^2}, \quad (7)$$

and the shift angle ϕ_s is calculated using

$$\phi_s(\Delta u', \Delta v') = \begin{cases} \arctan(\frac{\Delta v'}{\Delta u'}), & \text{if } \Delta u' > 0, \Delta v' \geq 0 \\ \arctan(\frac{\Delta v'}{\Delta u'}) + 2\pi, & \text{if } \Delta u' > 0, \Delta v' < 0 \\ \arctan(\frac{\Delta v'}{\Delta u'}) + \pi, & \text{if } \Delta u' < 0 \\ \frac{\pi}{2}, & \text{if } \Delta u' = 0, \Delta v' > 0 \\ \frac{3\pi}{2}, & \text{if } \Delta u' = 0, \Delta v' < 0 \end{cases}, \quad (8)$$

where $\Delta u' = u'_n - u'_{n-m}$ and $\Delta v' = v'_n - v'_{n-m}$, respectively.

Thus, between two sequential chromaticities P_n and P_{n-m} determined for an LED, whose maintenance measurements were segregated by a time interval $\Delta t = t_n - t_{n-m}$, the corresponding shift vector $\mathrm{SV}(\Delta t) = (r_s(\Delta t), \phi_s(\Delta t))^T$ can

be constructed. Calculating each SV for a given time series of chromaticity coordinates eventually yields a $\Delta_{u'v'}(t)$-diagram with additional angular information. The latter can be used to classify the individual shift directions for CSM analysis by categorizing them into one of the four possible shift regions (SR), i.e., blue, green, yellow, and red. However, as the origin of the polar coordinate system varies with time, a simple mapping $\phi_s \in [0°, 360°) \mapsto \mathrm{SR} \in [\text{blue}, \text{green}, \text{yellow}, \text{red}]$ would introduce unacceptably large inaccuracies. To eliminate these inaccuracies further steps must be taken. However, before the actual chromaticity shift evaluation can be performed, some auxiliary steps are required and should be discussed accordingly.

A. Auxiliary Steps

a) Shift function: A linear function of the form $v' = f_{\mathrm{CS}}(u') = mu' + b$ with $m = \frac{v'_n - v'_{n-m}}{u'_n - u'_{n-m}}$ and $b = v'_n - mu'_n$ is adopted for extrapolating the SV towards the spectral locus of the CIE 1976 (u', v') diagram. Making use of the respective intercept for subsequent SR determination ensures more accurate results.

b) Create spectral locus vector set: The spectral locus is obtained by applying Eqs. (1)–(3) to (relative) monochromatic stimuli of the form

$$S_{\lambda_i}(\lambda) = \begin{cases} 1 & \lambda = \lambda_i \\ 0 & \text{otherwise} \end{cases}, \tag{9}$$

where $\lambda_i \in [380\,\mathrm{nm}, 780\,\mathrm{nm}]$, resulting in a set of corresponding tristimulus values $X_{\lambda_i} = K\bar{x}(\lambda_i)$, $Y_{\lambda_i} = K\bar{y}(\lambda_i)$, and $Z_{\lambda_i} = K\bar{z}(\lambda_i)$. Inserting those terms into Eqs. (4) and (5) eventually yields the desired set of spectral locus coordinates

$$\begin{aligned} P_{\lambda_i} &= \begin{pmatrix} u'_{\lambda_i} \\ v'_{\lambda_i} \end{pmatrix} \\ &= \begin{pmatrix} \frac{4X_{\lambda_i}}{X_{\lambda_i}+15Y_{\lambda_i}+3Z_{\lambda_i}} \\ \frac{9Y_{\lambda_i}}{X_{\lambda_i}+15Y_{\lambda_i}+3Z_{\lambda_i}} \end{pmatrix} \\ &= \begin{pmatrix} \frac{4\bar{x}(\lambda_i)}{\bar{x}(\lambda_i)+15\bar{y}(\lambda_i)+3\bar{z}(\lambda_i)} \\ \frac{9\bar{y}(\lambda_i)}{\bar{x}(\lambda_i)+15\bar{y}(\lambda_i)+3\bar{z}(\lambda_i)} \end{pmatrix}. \end{aligned} \tag{10}$$

c) Define affiliation area: Since the coordinate of the intercept $P_\cap$ may be located between two neighboring spectral locus coordinates, e.g., P_{λ_i} and $P_{\lambda_{i-1}}$ or P_{λ_i} and $P_{\lambda_{i+1}}$, an affiliation area around each P_{λ_i} has to be defined to make a proper wavelength assignment. For this purpose, a rectangular area with boundaries $u'_{\lambda_i} \pm \Delta u'_\pm$ and $v'_{\lambda_i} \pm \Delta v'_\pm$ is defined for each P_{λ_i} (c.f. Fig. 2), where

$$\begin{aligned} \Delta u'_+ &= 0.5\left(u'_{\lambda_{i+1}} - u'_{\lambda_i}\right) \\ \Delta u'_- &= 0.5\left(u'_{\lambda_i} - u'_{\lambda_{i-1}}\right) \\ \Delta v'_+ &= 0.5\left(v'_{\lambda_{i+1}} - v'_{\lambda_i}\right) \\ \Delta v'_- &= 0.5\left(v'_{\lambda_i} - v'_{\lambda_{i-1}}\right) \end{aligned}. \tag{11}$$

d) Define Shift Regions: If the intercept $P_\cap$ is located within the affiliation area of the spectral locus coordinate P_{λ_i}, a corresponding intersection wavelength $\lambda_\cap = \lambda_i$ will be assigned, which can subsequently be used for SR categorization:

$$\mathrm{SR}(\lambda_\cap) \begin{cases} \text{Blue}, & \text{if } \lambda_\cap \in [380\,\mathrm{nm}, 480\,\mathrm{nm}) \\ \text{Green}, & \text{if } \lambda_\cap \in [480\,\mathrm{nm}, 560\,\mathrm{nm}) \\ \text{Yellow}, & \text{if } \lambda_\cap \in [560\,\mathrm{nm}, 620\,\mathrm{nm}) \\ \text{Red}, & \text{if } \lambda_\cap \in [620\,\mathrm{nm}, 780\,\mathrm{nm}] \end{cases}, \tag{12}$$

where the individual shift direction intervals have been defined according to [21].

B. Determination of Intersection Wavelength and Shift Region

With the auxiliary steps discussed in the previous section, the proposed chromaticity shift evaluation method is in principle based on the more or less straightforward determination of the intercept $P_\cap$. Five different algorithmic approaches should be presented in the following and compared with regard to their accuracy and performance: i) Analytical calculation, ii) Trial-and-Error, iii) Gamut crossing, iv) least differences and v) valid angles.

a) Analytical calculation: This approach is intended to find an exact analytical solution for the intercept $P_\cap$ between the spectral locus $f_{\mathrm{locus}}(u')$ and the extrapolation function $f_{\mathrm{CS}}(u')$. Due to the ambiguous nature of the former with a single minimum in the u' coordinate at $u' = u'_{\lambda_i}$ for $\lambda_i = 504\,\mathrm{nm}$, the vector set of spectral locus coordinates of Eq. (10) must be divided into two distinct subsets, one for $\lambda_i \in L_1 = [380\,\mathrm{nm}, 504\,\mathrm{nm})$ and the other for $\lambda_i \in L_2 = [504\,\mathrm{nm}, 780\,\mathrm{nm}]$. This basically yields two bijective functions $f_{L_1}(u')$ and $f_{L_2}(u')$ that can now be used for describing the lower and the upper part of the spectral locus separately.

In addition, the spectral locus' purple boundary, which is represented by a straight connection line between the spectral locus coordinates for $\lambda_i = 380\,\mathrm{nm}$ and $\lambda_i = 780\,\mathrm{nm}$, defines a possible third intersection function $f_{\mathrm{Purple}}(u')$ (c.f. Table II). To determine which intersection function to use, algorithm 1 can be applied.

Algorithm 1 Vector subset selection

$\phi_{380} \leftarrow \phi_s(P_{n-m}, P_{\lambda=380\,\mathrm{nm}})$
$\phi_{504} \leftarrow \phi_s(P_{n-m}, P_{\lambda=504\,\mathrm{nm}})$
$\phi_{780} \leftarrow \phi_s(P_{n-m}, P_{\lambda=780\,\mathrm{nm}})$
if $\phi_{504} \le \phi_s(\Delta t) < \phi_{380}$ **then**
  return Subset 1
else if $\phi_{780} \le \phi_s(\Delta t) < \phi_{504}$ **then**
  return Subset 2
else if $\phi_{780} \le \phi_s(\Delta t) < \phi_{380}$ **then**
  return Purple Boundary
end if

Thus, depending on the direction of the observed chromaticity shift, algorithm 1 yields an analytical expression for the spectral locus $f_{\text{locus}}(u')$ that can subsequently be used to determine the intercept $P_\cap = f_{\text{CS}} \cap (f_{L_1} \veebar f_{L_2} \veebar f_{Purple})$. Once the coordinates of the intercept $P_\cap$ are known, its assignment to a certain affiliation area can be performed as described in Sec. IV-A in order to determine the corresponding intersection wavelength $\lambda_\cap$. Finally, applying Eq. (12) yields the exact shift direction $\text{SR}(\lambda_\cap)$.

b) Trial-and-error: The second approach that should be discussed here simply checks if $f_{\text{CS}}(u')$ intersects the boundaries of a given affiliation area belonging to P_{λ_i}. Thus, the corresponding algorithm 2 iterates over all spectral locus wavelengths $\lambda_i \in L_1 \veebar L_2$ and searches for potential crossings of $f_{\text{CS}}(u')$ with the outer affiliation area boundaries defined by the coordinate vectors $(u'_{\lambda_i,\min}, v'_{\lambda_i,\min})^T$ and $(u'_{\lambda_i,\max}, v'_{\lambda_i,\max})^T$, respectively. These coordinates are given by

$$\begin{aligned} u'_{\lambda_i,\min} &= u'_{\lambda_i} - \Delta u'_-, \\ u'_{\lambda_i,\max} &= u'_{\lambda_i} + \Delta u'_+, \\ v'_{\lambda_i,\min} &= v'_{\lambda_i} - \Delta v'_-, \\ v'_{\lambda_i,\max} &= v'_{\lambda_i} + \Delta v'_+. \end{aligned} \tag{13}$$

Note that in the unlikely event that the extrapolation function $f_{\text{CS}}(u')$ crosses multiple affiliation areas, for example in case that the shift origin is very close to the spectral locus, the first identified intersection will be returned. The intersection wavelength $\lambda_\cap = \lambda_i$ again determines the shift direction $\text{SR}(\lambda_\cap)$. If no intersection can be identified at all, a crossing with the purple locus is assumed.

Algorithm 2 Affiliation area edge crossing

```
for all λ_i ∈ L_1 ⊻ L_2 do
    u'_{λ_i,min} ← u'_{λ_i} − Δu'_−
    u'_{λ_i,max} ← u'_{λ_i} + Δu'_+
    v'_{λ_i,min} ← v'_{λ_i} − Δv'_−
    v'_{λ_i,max} ← v'_{λ_i} + Δv'_+
    if v'_{λ_i,min} < f_CS(u'_{λ_i,min}) ≤ v'_{λ_i,max} or
       v'_{λ_i,min} < f_CS(u'_{λ_i,max}) ≤ v'_{λ_i,max} or
       u'_{λ_i,min} < f_CS^{-1}(v'_{λ_i,min}) ≤ u'_{λ_i,max} or
       u'_{λ_i,min} < f_CS^{-1}(v'_{λ_i,max}) ≤ u'_{λ_i,max} then
       return SR(λ_i)
    else
       if λ_i is 780 nm then
          return Purple
       end if
    end if
end for
```

c) Gamut Crossing: Gamut crossing represents a very efficient method, if one is only interested in obtaining a robust estimate of SR rather than calculating the exact intersection wavelength $\lambda_\cap$ first. For this method, a gamut is spanned within the CIE 1976 (u', v') diagram by connecting the wavelength boundaries of each SR defined in Eq. (12) with straight line segments (c.f. Fig. 2). Each line segment is then expressed in terms of a linear function $f_{\text{SR}}(u') = m_{\text{SR}} \cdot u' + b_{\text{SR}}$, where the function parameters m_{SR} and b_{SR} are summarized in Table II for all five possible shift directions.

TABLE II
LINEAR FUNCTIONS REPRESENTING EACH EDGE OF THE SPANNED GAMUT BETWEEN CORNER WAVELENGTHS OF THE DIFFERENT SHIFT REGIONS.

$f_{\text{SR}}(u')$	SR	λ_1 in nm	λ_2 in nm	m_{SR}, b_{SR}
$f_{\text{Blue}}(u')$	Blue	380	479	-1.43390295972, 0.3847963123139
$f_{\text{Green}}(u')$	Green	480	559	4.650202284955, -0.1142479099392
$f_{\text{Yellow}}(u')$	Yellow	560	619	-0.148902112296, 0.5993799077367
$f_{\text{Red}}(u')$	Red	620	780	-0.149495372891, 0.584519144337
$f_{\text{Purple}}(u')$	Purple	780	380	1.33701857218, 0.48446562958

SR can then be evaluated by calculating the intersections between each line segment $f_{\text{SR}}(u')$ and the linear extrapolation function $f_{\text{CS}}(u')$ of the observed chromaticity shift. The corresponding calculation steps are shown in Algorithm 3.

Algorithm 3 Gamut edge crossing

```
for all f_SR do
    u'_∩ ← (b_CS − b_SR) / (m_SR − m_CS)
    if u'_CS(λ_1) < u'_∩ ≤ u'_CS(λ_2) then
        v'_∩ ← f_CS(u'_∩)
        if v'_CS(λ_1) < v'_∩ ≤ v'_CS(λ_2) then
            return SR
        end if
    end if
end for
```

d) Least Differences: As a fourth method, it is also possible to determine the intersection wavelength $\lambda_\cap$ and, thus, the SR in a least-squares manner. Again, a spectral locus subset has to be chosen first by applying algorithm 1 in order to avoid obtaining the complementary wavelength as a false result. Based on the selected subset, a least-squares search algorithm can then be applied. Searching for the spectral locus wavelength λ_i that gives a minimal distance between v'_{λ_i} and the chromaticity shift extrapolation function value $f_{\text{CS}}(u'_{\lambda_i})$ automatically yields the corresponding intersection wavelength, i.e.,

$$\min_{\lambda_i \in L_1 \veebar L_2} \left| f_{\text{CS}}(u'_{\lambda_i}) - v'_{\lambda_i} \right| \longrightarrow \lambda_\cap \tag{14}$$

e) Valid Angles: Similar to algorithm 1, two additional angles ϕ_{λ_i} and $\phi_{\lambda_{i+1}}$ can be calculated between the origin P_{n-m} and the two consecutive spectral locus wavelength

coordinate vectors P_{λ_i} and $P_{\lambda_{i+1}}$, respectively. Iterating λ_i over the spectral locus wavelength range until the condition $\phi_{\lambda_i} \leq \phi_s(\Delta t) < \phi_{\lambda_{i+1}}$ is met automatically yields the intersection wavelength $\lambda_\cap = \lambda_i$, from which SR can again be determined. Algorithm 4 summarizes this approach.

Algorithm 4 Valid angles approach

```
for all λ_i ∈ [380 nm, 780 nm] do
    φ_{λ_i} ← φ_s(P_{n−m}, P_{λ_i})
    φ_{λ_{i+1}} ← φ_s(P_{n−m}, P_{λ_{i+1}})
    if φ_{λ_{i+1}} ≤ φ_s(Δt) < φ_{λ_i} then
        return SR(λ_i)
    end if
    if λ_i is 780 nm then
        return Purple
    end if
end for
```

V. Application Example

In order to evaluate the proposed methodology for collecting and reporting chromaticity maintenance data with a performance testing of the different algorithms, a set of 1000 randomly generated chromaticity coordinates P with $u' \in [0.1, 0.4]$ and $v' \in [0.3, 0.5]$ is used for this purpose. Each of these so constructed data points is considered to represent a separate measurement in time. Compared to real LED lifetime data, this artificial data set shows a considerably larger variance and, thus, allows for a more thorough performance analysis regarding generalizability. A python implementation of the different algorithms including the evaluation data are available for download from the university's *research repository*.

Following the procedure discussed in Sec. IV, the relative shift vectors SV_n of the evaluation data are calculated first by using Eqs. (7) and (8), respectively. For illustrative purposes, Fig. 1 shows the corresponding shift distances and angles of the first ten entities with their CIE 1976 (u', v') chromaticity coordinates being additionally depicted in the inset. These shift representations can subsequently be used to determine the shift extrapolation functions $f_{\mathrm{CS},n}$ for an automated extraction of information on shift direction and intersection wavelength by applying the different evaluation algorithms.

Concerning the *Analytical Approach*, no satisfying fit functions for $f_{L_1}(u')$ and $f_{L_2}(u')$ have been found yet. In particular, an insufficient accuracy must be reported for the current implementation at the edges of these curve segments, which basically makes them unsuitable for being used in their present form. In addition, with the CIE colorimetry being defined only for a maximum spectral resolution of 1 nm, it is not expected that the "more exact" analytical solution would yield an increased benefit over the other methods with respect to CSM analysis.

Fig. 2 thus demonstrates the results of the *Trial-and-Error*, *Gamut Crossing* and *Valid Angles* methods as obtained for a single extrapolation function $f_{\mathrm{CS},k}(u')$, whereas the results of the *Least Differences* optimization are shown in Fig. 3. As can be seen, all four non-analytical approaches yield consistent results with regard to the determination of shift direction and intersection wavelength for this example. However, for

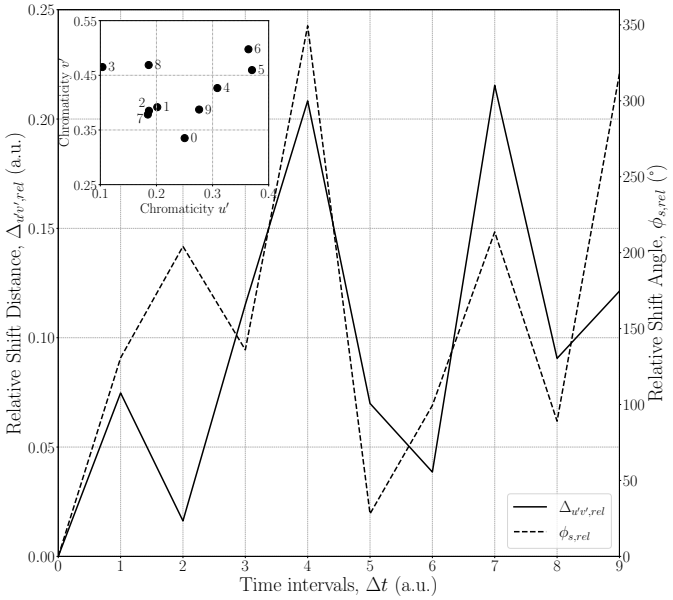

Fig. 1. Time dependence of the relative shift distance (solid line) and shift angle (dashed line) of the first ten data points of the evaluation data set. For each entity at time t_n, the indicated shift metrics are calculated relative to its predecessor at t_{n-1}. In addition, the corresponding CIE 1976 (u', v') chromaticity coordinates are depicted in the upper left inset.

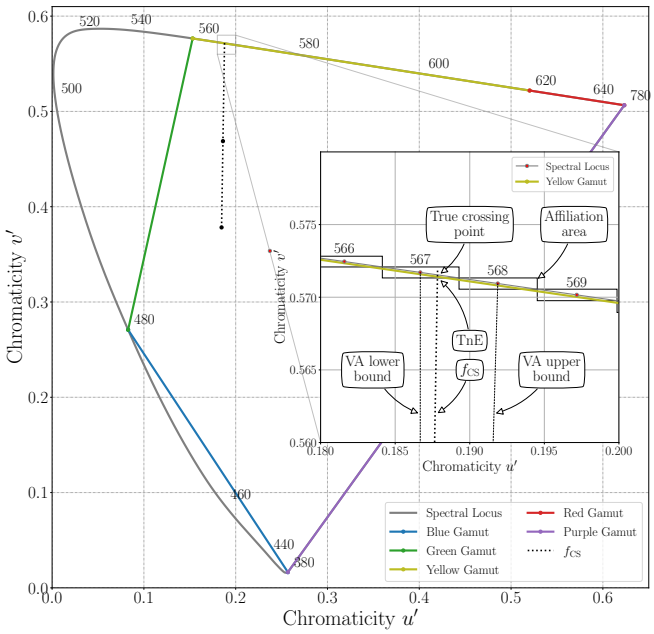

Fig. 2. Exemplary shift function $f_{\mathrm{CS},k}$ of the kth data point in the evaluation data set intersecting the spectral locus within the CIE 1976 (u', v') chromaticity diagram. The magnified area illustrates the determination of the corresponding intersection wavelength using *Trial-and-Error*, *Gamut Crossing* and *Valid Angles*, respectively.

TABLE III
ESTIMATED MEAN EXECUTION TIMES OF THE DIFFERENT ALGORITHMS FOR THE DATA POINTS IN THE EVALUATION DATA SET.

Approach	t_{mean}[ms]	t_{var}[ms]	Variance [%]	time factor
Trial-and-Error	4.636	0.014	0.3	1.4
Gamut Crossing	8.908	0.029	0.3	2.8
Least Differences	3.225	0.006	0.1	1.0
Valid Angles	164.777	17.36	11.7	51.1

a comprehensive performance analysis in terms of run time, accuracy, and ease of implementation, further considerations on a much broader base are required.

Here, run time is estimated by applying the different algorithms to the entire evaluation data set, while measuring the execution and processing times for each data point of the sequence. The resulting means and variances are shown in Table III. As can be seen, run time significantly increases for the *Valid Angles* approach compared to the other non-analytical methods. This finding can be explained by the computational time complexity of the $\arctan$ function used for the shift angle calculation, see Eq. (8), in combination with the large number of iterations over the spectral locus wavelength range required by the former.

In order to obtain an estimate for the (relative) accuracy of the non-analytical approaches, the different methods are compared in terms of their capability of properly predicting shift regions. By definition, *Valid Angles* can be considered as the most accurate approach since it always yields a unique solution for the intersection wavelength even at the edges of neighboring shift regions. On the contrary, *Trial-and-Error* and *Gamut Crossing* both may suffer from uncertainties in cases where the shift extrapolation function crosses two or more neighboring affiliation areas. For the *Least Differences* method, a source of error can be identified in the fact that it returns the first encountered minimum matching the optimization criterion even though there might be further minima to be evaluated.

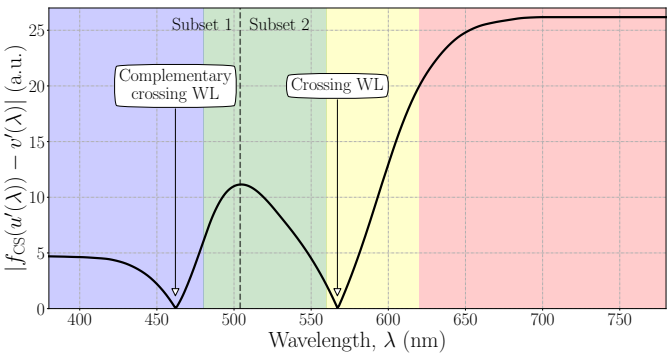

Fig. 3. Approximation behavior of the *Least Differences* approach as observed for an exemplary single shift function $f_{\mathrm{CS},k}$. Both minima indicate a crossing of the spectral boundary. In this case, the second wavelength subset was identified as being suitable for the determination of the proper intersection wavelength. Thus, the first minimum indicates the complementary and the second minimum the desired intersection wavelength. Note that the background is colored according to the previously defined shift regions SR for a better visualization of the wavelength assignment.

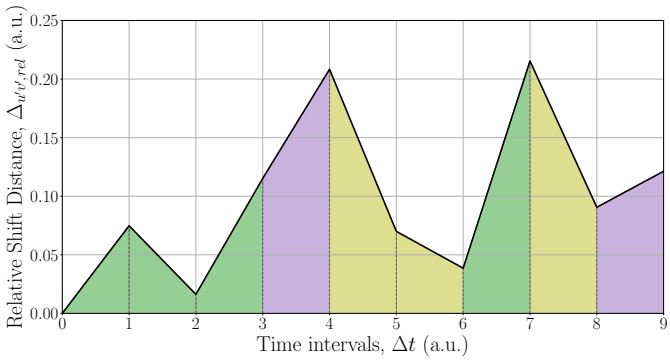

Fig. 4. Combined evaluation of chromaticity shift direction and distance. For each measurement time interval Δt, the assigned shift region is visualized by representative color coding.

Thus, taking *Valid Angles* as the corresponding reference, accuracy analysis performed on the complete evaluation data set revealed that the results obtained for both *Trial-and-Error* and *Least Differences* match in more than 99 % of the executed calculations with those obtained for the *Valid Angles* approach. In contrast, the outputs of the *Gamut Crossing* method match only in 70 % of the cases. Based on these findings, it can be concluded that *Trial-and-Error*, *Least Differences*, and *Valid Angles* provide an equally high accuracy, whereas significantly less accurate results must be expected for the *Gamut Crossing* approach.

Finally, the ease of implementation of the different methods should be analyzed. *Trial-and-Error* and *Gamut Crossing* both require the calculation of affiliation areas and, as a consequence, the definition of several linear functions. The evaluation of these functions to check for intersections yields a large number of necessary comparisons, which are a possible source of error during the implementation process. *Least Differences*, on the other hand, is based on a finite number of re-occurring calculations on a table- or array-like data structure. Software packages specifically optimized for those data structures, e.g., NumPy or Pandas for python, provide a simple and fast implementation due to an intuitive level of abstraction. An even higher ease of implementation must be concluded for the *Valid Angles* approach as it basically computes and compares only three different vector angles ϕ_{λ_i}, $\phi_{\lambda_{i+1}}$, and $\phi_s(\Delta t)$, respectively. In most programming languages this kind of calculation is provided by core software packages as a standard feature.

Fig. 4 eventually summarizes the time-dependent chromaticity shift characterization by means of its distance $\Delta_{u'v'}(\Delta t)$ and associated shift region $\mathrm{SR}(\Delta t)$ as proposed in this work. Again, only the results obtained for the first ten entities of the evaluation data set are shown for illustrative purposes. Note that the *Least Differences* approach has been used to perform the calculations. For each measurement time interval Δt, the corresponding shift region is visualized by representative color coding.

VI. Conclusion

In this paper, an enhanced methodology for displaying and classifying time-dependent chromaticity shifts of LEDs has been presented. Five different algorithms for implementation were discussed and their performance was compared in terms of run time, prediction accuracy and ease of implementation. The *Analytical Approach* was excluded due to unacceptable inaccuracies in the functional description of the different spectral locus segments of the CIE 1976 (u', v') diagram. Of the four remaining non-analytical approaches, the *Least Differences* method performed best in terms of accuracy, run time and ease of implementation. The *Trial-and-Error* method offers a good run time performance but essentially lacks in ease of implementation. The *Valid Angles* approach shows, by definition, the highest accuracy but also exhibits the largest drawback in terms of run time. *Gamut Crossing*, on the other hand, failed in terms of accuracy compared to the other approaches. Thus, it can be concluded that the *Least Differences* method shows the best overall performance and, consequently, constitutes the recommended algorithm to be applied for enhanced chromaticity shift evaluation of LEDs and related products.

Furthermore, it should be noted that the presented methodology can be adapted with little effort regarding the shift regions as well as their wavelength ranges. Thus, it is theoretically possible to represent any change of two color impressions that can be displayed in the CIE 1976 (u', v') UCS color space. This includes not only light sources such as LEDs, incandescent lamps or fluorescent lamps, but also, for example, changes in the reflectance or transmittance of objects.

Acknowledgment

The authors would like to thank the Federal Ministry for Economic Affairs and Energy (BMWi) for project IGF Nr. 19278 N, in the framework of which this publication was created.

References

[1] E. F. Schubert, J. K. Kim, H. Luo, and J. Xi, "Solid-state lighting–A benevolent technology," *Reports on Progress in Physics*, vol. 69, no. 12, pp. 3069–3099, 2006.

[2] J. Li, J. Wang, X. Yi, Z. Liu, T. Wei, J. Yan, and B. Xue, "Applications of LEDs," in *III-Nitrides Light Emitting Diodes: Technology and Applications*. Singapore: Springer, 2020, pp. 229–251.

[3] H. Wachta and P. Bojda, "Usability of luminaries with LED sources to illuminate the window areas of architectural objects," in *Proceedings of the 13th Selected Issues of Electrical Engineering and Electronics (WZEE)*. Rzeszow, Poland: IEEE, 2016.

[4] A. Bielawny, T. Schupp, and C. Neumann, "Automotive lighting continues to evolve," *Optics and Photonics News*, vol. 27, no. 11, pp. 36–43, 2016.

[5] B. Gayral, "LEDs for lighting: Basic physics and prospects for energy savings," *Comptes Rendus Physique*, vol. 18, no. 7–8, pp. 453–461, 2017.

[6] C. Sun, X. Lee, I. Moreno, C. Lee, Y. Yu, T. Yang, and T. Chung, "Design of LED street lighting adapted for free-form roads," *IEEE Photonics Journal*, vol. 9, no. 1, p. 8200213, 2017.

[7] K. M. Zielinska-Dabkowska and K. Xavia, "Historic urban settings, LED illumination and its impact on nighttime perception, visual appearance, and cultural heritage identity," in *Proceedings of the 5th International Multidisciplinary Scientific Conference on Social Sciences and Arts*. Florence, Italy: STEF92 Technology Ltd., 2018, pp. 277–291.

[8] L. Sipos, I. F. Boros, L. Csambalik, G. Székely, A. Jung, and L. Balázs, "Horticultural lighting system optimalization: A review," *Scientia Horticulturae*, vol. 273, p. 109631, 2020.

[9] J. L. Richter, L. Tähkämö, and C. Dalhammar, "Trade-offs with longer lifetimes? The case of LED lamps considering product development and energy contexts," *Journal of Cleaner Production*, vol. 226, pp. 195–209, 2019.

[10] M. Hansen and L. Davis, "LED Luminaire Reliability : Impact of Color Shift," United States Department of Energy, Tech. Rep. April, 2017.

[11] M. H. Chang, D. Das, P. V. Varde, and M. Pecht, "Light emitting diodes reliability review," *Microelectronics Reliability*, vol. 52, no. 5, pp. 762–782, 2012.

[12] K. Paisnik, G. Rang, and T. Rang, "Life-time characterization of leds," *Estonian Journal of Engineering*, vol. 17, no. 3, pp. 241–251, 2011.

[13] ANSI/IES TM-21-19, "Technical Memorandum: Projecting Long Term Lumen, Photon, and Radiant Flux Maintenance of LED Light Sources," Illuminating Engineering Society, Tech. Rep., 2019.

[14] J. Hegedüs, G. Hantos, and A. Poppe, "Lifetime modelling issues of power light emitting diodes," *Energies*, vol. 13, no. 13, p. 3370, 2020.

[15] ANSI/IES LM-80-20, "Measuring Luminous Flux and Color Maintenance of LED Packages, Arrays, and Modules," 2020.

[16] P. Bodrogi, X. Guo, D. Stojanovic, S. Fischer, and T. Q. Khanh, "Observer preference for perceived illumination chromaticity," *Color Research and Application*, vol. 43, no. 4, pp. 506–516, 2018.

[17] T. Q. Khanh, P. Bodrogi, X. Guo, Q. T. Vinh, and S. Fischer, "Colour preference, naturalness, vividness and colour quality metrics, part 5: A colour preference experiment at 2000 lx in a real room," *Lighting Research and Technology*, vol. 51, no. 2, pp. 262–279, 2019.

[18] S. Fotios and R. Gibbons, "Road lighting research for drivers and pedestrians: The basis of luminance and illuminance recommendations," *Lighting Research and Technology*, vol. 50, no. 1, pp. 154–186, 2018.

[19] U.S. Environmental Protection Agency, "Program Requirements for Solid-State Lighting (SSL) Products," Tech. Rep., 2009. [Online]. Available: https://www.energystar.gov/ia/partners/product_specs/program_reqs/Solid-State_Lighting_Program_Requirements.pdf

[20] W. D. Van Driel and X. J. Fan, *Solid state lighting reliability Part 2: Components to systems*, volume 3 ed., G. Zhang and W. Ling, Eds. Springer International Publishing, 2018.

[21] J. Zwinkels, "Light, electromagnetic spectrum," *Encyclopedia of Color Science and Technology*, 2015.